INSTABILITY PHENOMENA OF A RECTANGULAR ELASTIC PLATE UNDER BENDING AND SHEAR

M. Nakazawa, T. Iwakuma and S. Kuranishi

Department of Civil Engineering, Faculty of Engineering, Tohoku University, Aoba Sendai 980, Japan

and

M. Hidaka

Bridge Design Section, NKK Corporation, Yokohama, Kanagawa, 230, Japan

Abstract—This paper focuses on the instability phenomena of an elastic rectangular plate under pure bending which emerge after the occurrence of the primary buckling. The mechanisms of this instability behavior are investigated phenomenally throughout the analysis of load-deflection simulations. The relationships between the characteristics of this instability and the boundary conditions of a plate are also discussed. The effect of initial deflections on the post-buckling paths and secondary instability phenomena is examined from the viewpoint of imperfection-sensitivity. Finally, it is presented that a plate also shows the similar instability phenomena when subjected to unequal bending and shear.

1. INTRODUCTION

It is well known that the initial or primary buckling of an elastic flat plate is generally a stable symmetric bifurcation from the initially undeflected equilibrium state. Such an elastic plate retains the sufficient rigidity even beyond the primary buckling point and shows stable and monotonical behavior in the post-buckling range.

As for the large deflection problems of the elastic plate, Levy (1942) solved von Kármán's fundamental equations in the case of a simply-supported square plate under edge compression combined with the lateral pressure. Numerical results for the large deflection problems are compared with some experimental load-deflection curves and the effective width formulae available. Coan (1951) solved Marguerre's fundamental equations with the effect of small initial curvature of a simply-supported plate to improve Levy's solution. It was assumed that the supporting edges are stress-free and the loading edges are uniformly displaced as the boundary conditions. Yamaki (1959) also solved Marguerre's fundamental equations under eight different boundary conditions which combine two kinds of loading conditions and four kinds of supporting conditions. The solutions by Levy and Coan can be obtained as special cases from these results.

From these studies, it has also been well known that the post-buckling behavior of a plate becomes complicated owing to the two-dimensional property which yields the highly-mixed harmonic patterns in the deformed configuration. Therefore, it is not surprising to have further instability phenomena of the elastic plates even after the primary buckling load.

In some experimental and theoretical studies on the post-buckling behaviors of a rectangular plate subjected to the in-plane uniaxial compression [e.g. Bauer and Reiss (1965), Supple (1967, 1968, 1970), Chilver (1967), Sharman and Humpherson (1968), and Uemura and Byon (1977, 1978)], it has been revealed that a plate deformed in a primary buckling mode may snap abruptly to another configuration with a different pattern of deflection. This phenomenon has been called the secondary instability or the secondary buckling of plates.

Supple (1970) investigated this sudden change of the wave-form of simply-supported rectangular plates under uniaxial compression using the 2 DOF characterized by the buckling modes. The effects of the boundary conditions at the unloaded edge and imperfections are also examined by considering the uncoupled and coupled buckling modes.

Nakamura and Uetani (1979) improved the theoretical investigation of the secondary buckling and post-secondary behaviors by the multi-term coupling effect of buckling modes. Unstable and stable symmetric bifurcation points on the secondary branching paths are observed, and the snap-through motions involving an abrupt change of wave-form are found to be possible.

Recently, Maaskant and Roorda (1992) studied the post-buckling behavior of a simply-supported plate under combined loading of biaxial compression. This interaction of loadings leads to the mode jumping phenomenon associated with the secondary bifurcation, and the characteristics of mode coupling in the buckling modes are described in several loading conditions.

A similar secondary instability phenomenon has been observed by Hasegawa et al. (1987) on the column with one end fixed and the other hinged, the so-called propped-cantilever column. Furthermore, Levy et al. (1945) and Konishi et al. (1966) investigated the post-buckling behavior of simply-supported webs under pure shear loading to simulate the formation of a tension field. The elastic post-buckling behavior of a rectangular plate under combined actions of compression and bending was studied by Usami (1982). An energy method is applied to solve Marguerre's equation, and this result is utilized to derive the effective width formulae.

However, none of them pointed out the existence of instability in the post-buckling behavior of elastic plates under bending or shear. Fujii and Ohmura (1989) reported that in the elastic FEM analysis of a panel of curved girders, some numerically unstable points exist at which a large number of iterations are required to obtain a converged answer. We believe that this is also the secondary instability phenomenon, but this kind of unstable mechanism of plates has not been focused on up to now. The objectives of this study are to trace this instability phenomenon in the post-buckling range and to reveal its mechanism and characteristics. An analytical approach is employed to simulate the load-deflection behavior.

As we are concerned with the behavior of a rectangular plate in the plate girder structures, a simply-supported plate and another one with two opposite sides clamped and the other two sides simply-supported are examined. In the latter model, the clamped sides express the effect of the flange plates and the simply-supported edges correspond to the vertical stiffeners of a web plate. Shearing forces on four sides and bending moments only on the simply-supported sides are applied, where both the equal and unequal bending moments are considered.

Moreover, since the effect of initial deflections on the equilibrium paths is the one we are interested in, we also examine the relationships between the initial imperfection and the instability phenomenon from a viewpoint of imperfection-sensitivity. These relations are examined by varying both the modes and magnitudes of the imperfections. Finally, we present a rectangular plate which also shows the instability phenomena due to the effect of combined loading when subjected to unequal bending and shear.

We here employ a classical but analytical approach to trace the equilibrium paths in the load-deflection behavior of an elastic plate. Marguerre's fundamental equations for the plate bending are solved by Galerkin's method. The advantages of this analytical method over the FEM are the calculation efficiency such as saving of memory and CPU time, rapid convergence of Newton–Raphson iterations even at the instability points, and easy handling of loading and unloading control. FEM needs a huge number of discretized elements to obtain sufficient accuracy for the similar analyses.

2. INSTABILITY OF A SIMPLY-SUPPORTED RECTANGULAR PLATE

2.1. Fundamental equation

Marguerre's equations for the plate bending with relatively large deflection are expressed in terms of the out-of-plane deflection $w(x, y)$, initial deflection $w_0(x, y)$ and the in-plane stress function $F(x, y)$ as

$$\nabla^4 w = \frac{t}{D}\left[\frac{\partial^2 F}{\partial y^2}\frac{\partial^2(w+w_0)}{\partial x^2} + \frac{\partial^2 F}{\partial x^2}\frac{\partial^2(w+w_0)}{\partial y^2} - 2\frac{\partial^2 F}{\partial x\,\partial y}\frac{\partial^2(w+w_0)}{\partial x\,\partial y}\right], \tag{1a}$$

$$\nabla^4 F = E\left\{\left[\frac{\partial^2(w+w_0)}{\partial x\,\partial y}\right]^2 - \frac{1}{2}\left[\frac{\partial^2(w+w_0)}{\partial x^2}\frac{\partial^2(w+w_0)}{\partial y^2} + \frac{\partial^2(w+w_0)}{\partial y^2}\frac{\partial^2(w+w_0)}{\partial x^2}\right]\right.$$

$$\left. - \left(\frac{\partial^2 w_0}{\partial x\,\partial y}\right)^2 + \frac{1}{2}\left[\frac{\partial^2 w_0}{\partial x^2}\frac{\partial^2 w_0}{\partial y^2} + \frac{\partial^2 w_0}{\partial y^2}\frac{\partial^2 w_0}{\partial x^2}\right]\right\}, \tag{1b}$$

where t and $D \equiv Et^3/12(1-v^2)$ are the plate thickness and the flexural rigidity of the plate, respectively. E is Young's modulus and v is Poisson's ratio. In order to ensure the symmetric order of differentiation in the series expansion, eqn (1b) is modified in some parts from that of the well-known type.

The in-plane stress components $\sigma_x(x, y)$, $\sigma_y(x, y)$ and $\tau_{xy}(x, y)$ are related to the Airy stress function $F(x, y)$ as

$$\sigma_x = \frac{\partial^2 F}{\partial y^2}, \qquad \sigma_y = \frac{\partial^2 F}{\partial x^2}, \qquad \sigma_{xy} = -\frac{\partial^2 F}{\partial x\,\partial y}. \tag{2}$$

This stress function $F(x, y)$ must be determined to satisfy the loading condition. We here consider a problem in which the plate is subjected to pure shearing stress τ_a and unequal bending moments [see Kutzelnigg (1978) and Nakazawa et al. (1991)] M_1 and M_2 at both sides as shown in Fig. 1(a). Then, the mechanical boundary conditions given by the stress resultant forces can be expressed as

$$M(x) = -t\int_0^b \sigma_x(x,y)\left(y - \frac{b}{2}\right)\mathrm{d}y, \tag{3a}$$

$$M_1 = M(x = 0), \quad M_2 = M(x = a),$$

$$\int_0^b \sigma_x\,\mathrm{d}y = 0, \qquad \text{along } x = 0, a, \tag{3b}$$

$$\sigma_y = 0, \qquad \text{along } y = 0, b, \tag{3c}$$

$$\tau_{xy} = -\tau_a, \qquad \text{along } y = 0, b. \tag{3d}$$

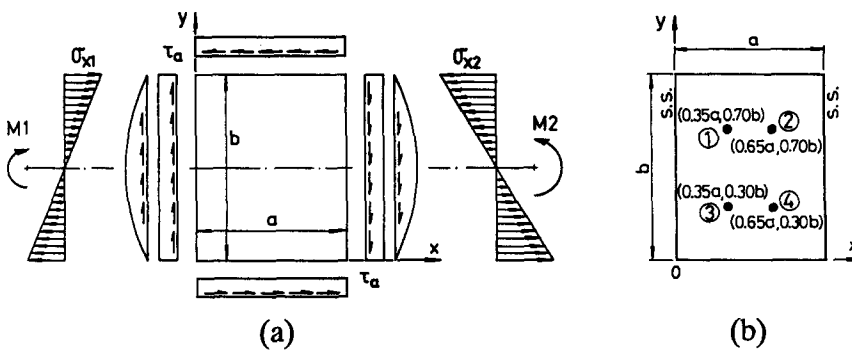These boundary conditions of eqns (3a)–(3d) can be exactly satisfied if

Fig. 1. Geometry of a rectangular elastic plate : (a) a panel subjected to unequal end moments and shearing force ; (b) observation points of out-of-plane deflection.

$$F_0(x,y) = \tau_a xy - \frac{y^2(2y-3b)}{b^3 t}\left[M_1 + (M_2 - M_1)\frac{x}{a}\right], \tag{4}$$

is chosen for the Airy stress function [see for example Timoshenko and Goodier (1970) or Nakazawa *et al.* (1991)] which is a homogeneous solution of eqn (1b).

The deflections can be expressed for the simply-supported condition of four edges as

$$w_0 = t \sum_{m=1}^{\infty} \sum_{n=1}^{\infty} a_{mn} \sin\left(\frac{m\pi x}{a}\right) \sin\left(\frac{n\pi y}{b}\right), \tag{5a}$$

$$w = t \sum_{m=1}^{\infty} \sum_{n=1}^{\infty} b_{mn} \sin\left(\frac{m\pi x}{a}\right) \sin\left(\frac{n\pi y}{b}\right), \tag{5b}$$

where a_{mn} are the given quantities of the initial deflection, and b_{mn} are the unknown coefficients to be determined. m and n are the number of half harmonic waves in the x- and y-directions, respectively.

The general expression of $F(x, y)$ is obtained by summing a particular solution corresponding to the right-hand side of eqn (1b) using eqn (5), and the homogeneous solution $F_0(x, y)$ of eqn (4) as

$$F(x,y) = F_0(x,y) + Et^2 \sum_{p=0}^{\infty} \sum_{q=0}^{\infty} \phi_{pq} \cos\left(\frac{p\pi x}{a}\right) \cos\left(\frac{2q\pi y}{b}\right). \tag{6}$$

In this case, the mechanical boundary condition of eqn (3c) must be relaxed to $\int_0^a \sigma_y \cdot dx = 0$. If eqn (3c) must be strictly satisfied, it is necessary to introduce additional terms (Usami, 1982) to eqn (6), but this function is expressed by a Fourier series which converges very slowly in the numerical calculation. Therefore, it is practically impossible to obtain the sufficient accuracy for the exact boundary condition of eqn (3c). Hence, we employed the relaxed one. Substituting eqns (5) and (6) into eqn (1b), we obtain the expression of ϕ_{pq} in terms of a_{mn} and b_{mn} as

$$\frac{8(p^2 + 4\alpha^2 q^2)^2}{\alpha^2} \phi_{pq} = \sum_{m=1}^{\infty} \sum_{n=1}^{\infty} \sum_{i=1}^{\infty} \sum_{j=1}^{\infty} (a_{mn}b_{ij} + b_{mn}a_{ij} + b_{mn}b_{ij})[2mnij \pm (m^2 j^2 + n^2 i^2)],$$

$$- :\begin{cases} p = m+i & \text{and } q = (n+j)/2 \\ \text{or} \\ p = |m-i| & \text{and } q = |n-j|/2 \end{cases} + :\begin{cases} p = |m-i| & \text{and } q = (n+j)/2, \\ \text{or} \\ p = m+i & \text{and } q = |n-j|/2, \end{cases} \tag{7}$$

where p and q are positive integers, and α is the aspect ratio of a panel, i.e. $\alpha \equiv a/b$. The final equation to be solved with eqn (7) can be obtained by direct substitution of eqns (5) and (6) into eqn (1a), but it becomes so complicated that Galerkin's method is applied to eqn (1a) in the form as

$$\int_0^a \int_0^b \left\{ \nabla^4 w - \frac{t}{D}\left[\frac{\partial^2 F}{\partial y^2} \frac{\partial^2(w+w_0)}{\partial x^2} + \frac{\partial^2 F}{\partial x^2} \frac{\partial^2(w+w_0)}{\partial y^2} - 2\frac{\partial^2 F}{\partial x \partial y} \frac{\partial^2(w+w_0)}{\partial x \partial y} \right] \right\}$$

$$\cdot \sin\left(\frac{r\pi x}{a}\right) \sin\left(\frac{s\pi y}{b}\right) dx\, dy = 0, \quad r, s = 1, 2, 3, \ldots. \tag{8}$$

By substituting eqns (5) and (6) into eqn (8) and integrating it, we obtain the following fundamental equations as a final form:

$$\frac{\pi^4}{4\alpha^2}(r^2+\alpha^2 s^2)^2 b_{rs} + 12(\lambda_2+\lambda_1)\sum_n{}' (a_{rn}+b_{rn})\frac{r^2 ns}{(n^2-s^2)^2}$$

$$+\frac{96}{\pi^2}(\lambda_2-\lambda_1)\sum_m{}'\sum_n{}' (a_{mn}+b_{mn})\frac{mnrs(r^2 s^2-m^2 n^2+3n^2 r^2-3m^2 s^2)}{(r^2-m^2)^2(s^2-n^2)^3}$$

$$+8\alpha\lambda_3\sum_m{}'\sum_n{}' (a_{mn}+b_{mn})\frac{mnrs}{(r^2-m^2)(s^2-n^2)} - \frac{3}{4}(1-v^2)\pi^4 \sum_{m=1}^{\infty}\sum_{n=1}^{\infty}(a_{mn}+b_{mn})$$

$$\cdot\{[m(n+s)-n(m+r)]^2\phi_{(m+r),(n+s)/2} - [m(n-s)-n(m+r)]^2\phi_{(m+r),(n-s)/2}$$

$$-[m(s-n)+n(m+r)]^2\phi_{(m+r),(s-n)/2} - [m(n+s)-n(m-r)]^2\phi_{(m-r),(n+s)/2}$$

$$+[m(n-s)-n(m-r)]^2\phi_{(m-r),(n-s)/2} + [m(s-n)+n(m-r)]^2\phi_{(m-r),(s-n)/2}$$

$$-[m(n+s)+n(r-m)]^2\phi_{(r-m),(n+s)/2} + [m(n-s)+n(r-m)]^2\phi_{(r-m),(n-s)/2}$$

$$+[m(s-n)-n(r-m)]^2\phi_{(r-m),(s-n)/2}\} = 0, \quad r,s = 1,2,3,\ldots, \tag{9}$$

where a prime on Σ indicates that the summation of m and n are taken only when $m\pm r$ or $n\pm s$ is odd. ϕ_{pq} are zero when $p < 0$ or $q < 0$, and the following non-dimensional parameters are introduced:

$$\lambda_1 \equiv \frac{M_1}{D}, \qquad \lambda_2 \equiv \frac{M_2}{D}, \qquad \lambda_3 \equiv \frac{\tau_a b^2 t}{D},$$

$$\gamma \equiv \frac{M_1}{M_2} = \frac{\lambda_1}{\lambda_2}, \qquad \omega \equiv \frac{\tau_a}{\sigma_{x2}} = \frac{\lambda_3}{6\lambda_2}, \tag{10}$$

where the parameters γ and ω are used to express the applied loading ratio of unequal bending moments and shearing force, respectively. σ_{x2} is the extreme fiber stress at $x = a$. Equation (9) results in a set of third-order simultaneous algebraic equations of b_{mn}, and the Newton–Raphson method is employed to solve it. Substitution of the obtained b_{mn}s into eqn (5b) yields the out-of-plane deflection in the post-buckling state.

2.2. Snap-through phenomena beyond primary buckling

A simply-supported rectangular plate subjected to only a pure bending moment is analysed here, i.e. $\lambda_1 = \lambda_2$ and $\lambda_3 = 0$ in eqn (10). Young's modulus E and Poisson's ratio v are 206 GN m^{-2} and 0.3, respectively. The out-of-plane deflections are observed at the four points as indicated in Fig. 1(b) so as to pick up the higher-order modes of deformation.

In order to check the truncation error of the series evaluation, the secondary buckling moments are compared with the solutions by Richardson's (h^2, h^4)-extrapolation formula [e.g. Salvadori (1951), Salvadori and Baron (1961), and Mikami and Yonezawa (1975)]. These results are shown in Fig. 2 and indicate that the infinite series can be truncated at m, $n = 6$ in the present analysis. In the same figure, another result to be used in Section 3 is
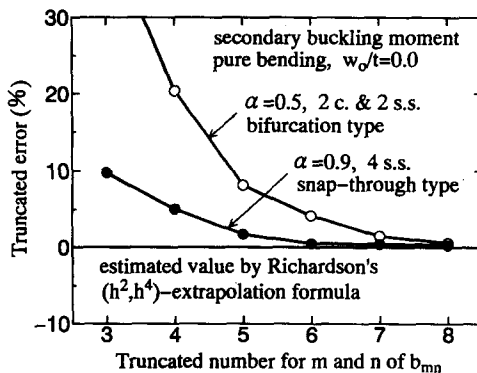

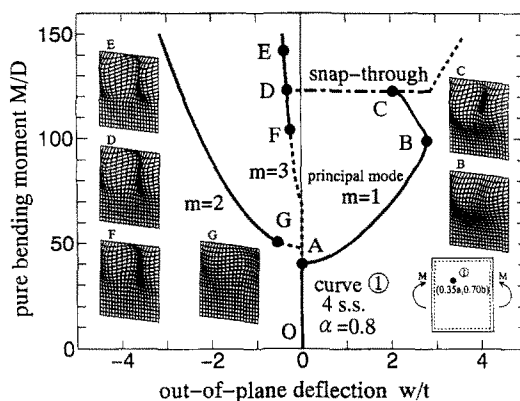Fig. 2. Accuracy check of analysis with respect to the secondary buckling moment.

Fig. 3. Typical post-buckling behavior of a simply supported plate under pure bending; *aspect ratio* $\alpha = 0.8$.

also shown by open circles within 5% error for the boundary condition of two opposite sides clamped and the other two sides simply supported.

Figure 3 shows a typical post-buckling behavior in the case of aspect ratio $\alpha = 0.8$. The load-deflection curves at the point $(0.35a, 0.70b)$ are plotted for different equilibrium states with respect to the principal mode m. In the same figure, the out-of-plane deformed configurations are shown at several characteristic points.

In this analysis, all equilibrium paths are obtained when the iterative calculation has converged regardless of the stability of that configuration. In order to check the stability, the sign of eigenvalues of the Jacobian matrix in the Newton–Raphson procedure must be examined [see for example Thompson and Hunt (1973, 1984) and Britvec (1973)]. Namely, the stable path is identified only when the Jacobian matrix is positive definite. Stable paths are drawn by solid lines, while broken lines represent the unstable ones. A dashed-and-dotted line indicates the abrupt change of equilibrium paths.

After reaching the primary buckling moment at point A, the out-of-plane deformation gradually begins to grow in the principal mode of $m = 1$, and other minor modes of $m = 3$, 5 also develop as the applied moment increases. The direction of out-of-plane deflection increment reverses at point B, and the snap-through phenomenon occurs from the point C to D. Here, the type of instability is determined phenomenally to be the snap-through as shown in the uniformly compressed plate [e.g. Nakamura and Uetani (1979)] or the shallow arch problems. At point C, the equilibrium path also jumps into another unstable one indicated by a broken line in the figure, but it does not continue smoothly from the preceding stable path. Consequently, the point C is a limit point in the same manner as the instability of the shallow arches or some of shell structures. It must be noticed that two symmetrical equilibrium paths of opposite sign surely exist after the snap-through phenomenon, but this figure includes only one of them.

The point D lies exactly on the path of principal and single mode of $m = 3$ (curve FDE). This equilibrium path of $m = 3$ is stable only in the range above the point F. We may expect that an unstable path surely exists between the point C and F by the analogy with the shallow arch. This path may be obtained by using the displacement-control or arc-length method, but our analytical method can not employ these techniques, and we cannot trace it.

Although another path of principal mode $m = 2$ also exists and is stable above the point G, this mode does not participate in the instability phenomenon from the path of $m = 1$ in the case of $\alpha = 0.8$. As a result, the possible equilibrium path can take only the course of $OABC \rightarrow DE$.

It is found that the mechanism of the snap-through phenomena can be interpreted as a mode change from $m = 1$ to $m = 3$ in the deformed configuration. In other words, the strain energy stored in the deformed plate of the mode $m = 3$ becomes smaller at the point D than that of $m = 1$ at the snap-through point C.
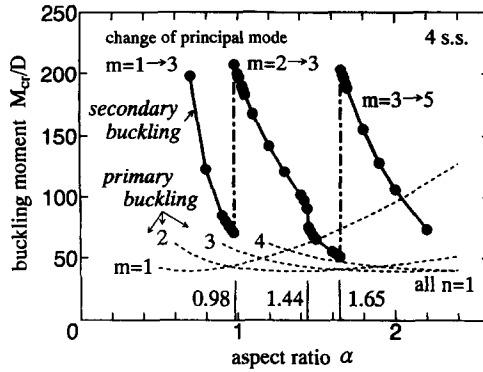
Fig. 4. Relationships between the snap-through secondary buckling moment and aspect ratio α under simply-supported condition; broken lines are the primary critical moments obtained by the linear analysis.

The relationships between the aspect ratio α of a panel and the secondary snap-through buckling moment are summarized in Fig. 4. This figure also includes the variation of the primary buckling moments which are obtained by the linear buckling analysis and are expressed by the broken lines. The secondary buckling moments indicated by solid lines become smaller and closer to the loading level of the primary ones near the conjunction points of the two adjacent primary buckling curves. This suggests that the secondary instability phenomenon is likely to occur in the practical situations of low loading level. However, these secondary buckling moments will never coincide with the primary buckling ones at the conjunction points of the primary buckling curves because of the effect of finite deflection prior to the buckling.

The variation of secondary buckling moment can be classified into three regions in the limited range of this analysis, and there will be other similar phenomena as the aspect ratio increases. While in the range of $\alpha \leqslant 0.98$ the secondary instability yields the mode change from $m = 1$ to 3, the change of mode from $m = 2$ to 3 occurs in the range of $0.98 < \alpha \leqslant 1.65$. Moreover in the latter case, the region is separated into two parts at $\alpha = 1.44$. This is because the composition of higher buckled mode is slightly different in these two parts, but the tendency of deformed configuration is almost the same. In the higher range of $\alpha > 1.65$, the mode of the secondary instability changes from $m = 3$ to 5.

2.3. Effect of initial deflection

Figure 5(a) shows the post-buckling paths for a plate of $\alpha = 0.8$ which has the initial deflection mode of a_{11} with variable magnitude of $0 \leqslant a_{11} \leqslant 1.0$. The number of n is fixed to unity for the sake of simplicity. The dashed line shows a stable fundamental path with
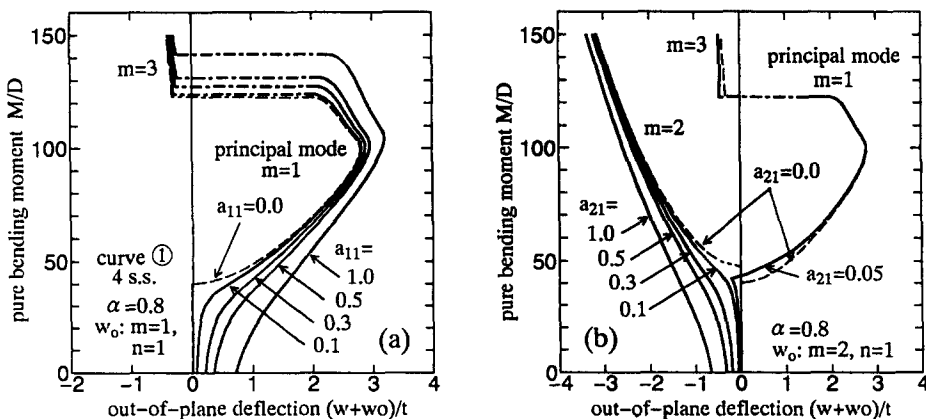

Fig. 5. Effect of initial deflection on a simply supported plate of *aspect ratio* $\alpha = 0.8$: (a) imperfection mode of a_{11} ; (b) a_{21}.

no imperfections. The larger the amplitude of initial deflection a_{11} becomes, the slightly higher the secondary buckling moment becomes. This result agrees with the report by Fujii and Ohmura (1989) that the numerically unstable load becomes higher as the curvature of a curved girder panel is larger.

The results become completely different when the initial deflection mode of a_{21} is chosen as in Fig. 5(b). This imperfection mode yields the governing effect on the following equilibrium paths to lead the stable and monotonical increasing behavior in most cases, but it depends on the magnitude of the a_{21} mode. Especially, when the initial deflection is very small such as $a_{21} = 0.05$, bifurcation occurs slightly after the initial buckling moment of $m = 1$, and the post-buckling path becomes similar to those with initial deflection mode of a_{11} as shown in Fig. 5(a). Although the figure is not shown, the initial mode of a_{31} has a similar stabilizing effect on the bifurcation phenomena as the imperfection mode of a_{21}. Another equilibrium path is also recognized in the case of $a_{31} = 0.1$ which is extensively affected by the mode of $m = 1$.

3. INSTABILITY OF A RECTANGULAR PLATE CLAMPED AT TWO OPPOSITE SIDES AND SIMPLY SUPPORTED ALONG THE OTHER TWO SIDES

3.1. *Fundamental equation*

The out-of-plane deflections are assumed to be given by the same shape function as those used by Moriwaki and Nara (1989) as

$$
w_0 = t \sum_{m=1}^{\infty} \sum_{n=1}^{\infty} a_{mn} \sin\left(\frac{m\pi x}{a}\right)\left\{\cos\left[\frac{(n-1)\pi y}{b}\right] - \cos\left[\frac{(n+1)\pi y}{b}\right]\right\}, \tag{11a}
$$

$$
w = t \sum_{m=1}^{\infty} \sum_{n=1}^{\infty} b_{mn} \sin\left(\frac{m\pi x}{a}\right)\left\{\cos\left[\frac{(n-1)\pi y}{b}\right] - \cos\left[\frac{(n+1)\pi y}{b}\right]\right\}. \tag{11b}
$$

In this case, the general expression of $F(x, y)$ is chosen as

$$
F(x,y) = F_0(x,y) + Et^2 \sum_{p=0}^{\infty} \sum_{q=0}^{\infty} \phi_{pq} \cos\left(\frac{2p\pi x}{a}\right)\cos\left(\frac{2q\pi y}{b}\right). \tag{12}
$$

Substituting eqns (11) and (12) into eqn (1b), we obtain the explicit expression for ϕ_{pq} as

$$
\sum_{p=0}^{\infty}\sum_{q=0}^{\infty} \frac{8[(2p)^2+\alpha^2(2q)^2]^2}{\alpha^2}\phi_{pq}C_x(2p)C_y(2q) = \sum_{m=1}^{\infty}\sum_{n=1}^{\infty}\sum_{i=1}^{\infty}\sum_{j=1}^{\infty}(a_{mn}b_{ij}+b_{mn}a_{ij}
$$

$$
+b_{mn}b_{ij})[-\{[m(j+1)-i(n-1)]^2+[m(j-1)-i(n+1)]^2\}C_x(m+i)C_y(n+j)
$$

$$
+[m(j+1)-i(n+1)]^2C_x(m+i)C_y(n+j+2)+[m(j-1)-i(n-1)]^2C_x(m+i)C_y(n+j-2)
$$

$$
+\{[m(j-1)+i(n-1)]^2+[m(j+1)+i(n+1)]^2\}C_x(m+i)C_y(n-j)
$$

$$
-[m(j-1)+i(n+1)]^2C_x(m+i)C_y(n-j+2)-[m(j+1)+i(n-1)]^2C_x(m+i)C_y(n-j-2)
$$

$$
+\{[m(j+1)+i(n-1)]^2+[m(j-1)+i(n+1)]^2\}C_x(m-i)C_y(n+j)
$$

$$
-[m(j+1)+i(n+1)]^2C_x(m-i)C_y(n+j+2)-[m(j-1)+i(n-1)]^2C_x(m-i)C_y(n+j-2)
$$

$$
-\{[m(j-1)-i(n-1)]^2+[m(j+1)-i(n+1)]^2\}C_x(m-i)C_y(n-j)
$$

$$
+[m(j-1)-i(n+1)]^2C_x(m-i)C_y(n-j+2)+[m(j+1)-i(n-1)]^2C_x(m-i)C_y(n-j-2)],
$$

$$
\tag{13}
$$

where

$$\mathbf{C}_x(\cdot) \equiv \cos\left[\frac{(\cdot)\pi x}{a}\right] \quad \text{and} \quad \mathbf{C}_y(\cdot) \equiv \cos\left[\frac{(\cdot)\pi y}{b}\right].$$

Similar to eqn (8), Galerkin's method is employed to solve eqn (1a) in the form

$$\int_0^a \int_0^b \left\{ \nabla^4 w - \frac{t}{D}\left[\frac{\partial^2 F}{\partial y^2}\frac{\partial^2(w+w_0)}{\partial x^2} + \frac{\partial^2 F}{\partial x^2}\frac{\partial^2(w+w_0)}{\partial y^2} - 2\frac{\partial^2 F}{\partial x\,\partial y}\frac{\partial^2(w+w_0)}{\partial x\,\partial y} \right] \right\}$$

$$\cdot \sin\left(\frac{r\pi x}{a}\right) [\mathbf{C}_y(s-1) - \mathbf{C}_y(s+1)] \, dx\, dy = 0, \quad r,s = 1,2,3,\ldots. \quad (14)$$

By substituting eqns (11) and (12) into eqn (14) and integrating it, we obtain the fundamental equations in the same manner as eqn (9). This also results in a set of third-order simultaneous algebraic equations of b_{mn}.

3.2. Bifurcation phenomena beyond primary buckling

Figure 6(a) shows the post-buckling path of a panel subjected to pure bending in the case of $\alpha = 0.5$ after the primary buckling with mode $m = 1$. This value of the aspect ratio is chosen so that the number of the primary buckling mode becomes almost the same as that of the simply-supported case with $\alpha = 0.8$. The encircled numerals indicate the observation points of out-of-plane deflection in Fig. 1(b). The stable equilibrium path of which configuration is composed of principal mode $m = 1$ with other minor modes 3, 5 starts at the primary bifurcation point A and goes up gradually to point C. This equilibrium path suddenly becomes unstable just above this point C and bifurcates to another stable path. After the instability occurs, all the harmonics of the b_{mn}s contribute to the deformation of a plate, but the principal mode remains $m = 1$, and the rate of these contributions becomes smaller as the order of the mode becomes higher. The symmetrical deformed configuration (point C) before the bifurcation changes into the asymmetrical ones (point D) after the bifurcation.

Figure 6(b) shows the case of $\alpha = 0.8$ in which the primary buckling mode is $m = 2$. In the post-buckling range, the principal mode of $m = 2$ and another minor mode of $m = 6$ also develop before the instability point C is reached. Although all the components of the b_{mn}s contribute to the deformation after the instability point, these contributions are in inverse proportion to the order of the mode, and the principal mode of $m = 2$ is still dominant.
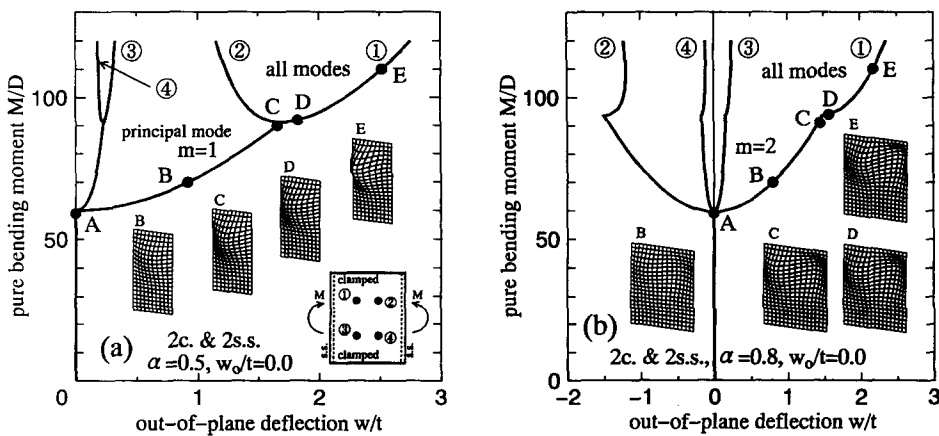

Fig. 6. Post-buckling behavior of a plate clamped at two opposite sides and simply supported along the other two sides under pure bending: (a) aspect ratio $\alpha = 0.5$; (b) $\alpha = 0.8$.
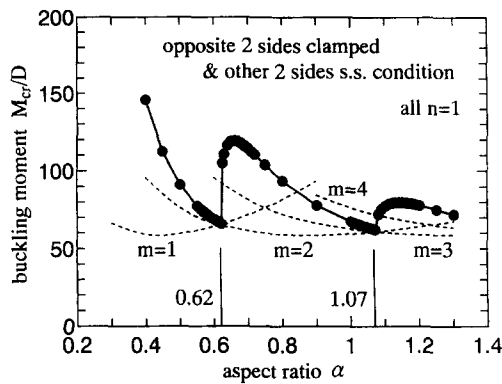
Fig. 7. Relationships between the secondary bifurcation moment and aspect ratio α under two opposite sides clamped and the other two sides simply supported condition.

The relationships between the aspect ratio α and the secondary buckling moment are summarized in Fig. 7 together with the plot of primary buckling loads which are obtained by the linear buckling analysis using the same shape function as eqn (11b). The variation of secondary buckling curve can be classified into three regions of $\alpha \leqslant 0.62$, $0.62 < \alpha \leqslant 1.07$ and $1.07 < \alpha$ in the limited range of this analysis. After reaching the instability point, all the harmonics of the b_{mn}s arise in the out-of-plane deformation, but the primary buckling mode remains.

The secondary buckling occurs almost at the same level as the primary buckling load when the aspect ratio approaches the conjunction points of the primary buckling curves at which the mode of primary buckling changes to the higher one. Therefore, this kind of secondary buckling is most likely to happen in the practical situations.

3.3. Effect of initial deflection

Figure 8(a) shows the post-buckling behavior for a panel of $\alpha = 0.5$ when the initial deflection of a_{11} is given with variable magnitude. The number of n is also fixed at unity for the sake of simplicity. The dashed line shows a stable fundamental path with no imperfections. Since the initial deflection mode of a_{11} coincides with the primary buckling mode, the primary buckling does not happen, but the secondary buckling occurs at a higher loading level. The mixed deformation modes of $m = 1, 3$ and 5 develop into all the harmonics of the b_{mn}s after reaching the bifurcation point, while the principal mode of $m = 1$ still remains. The amplitude of the initial deflection serves to increase the secondary buckling moment as has been observed in the case of the simply-supported boundary condition.
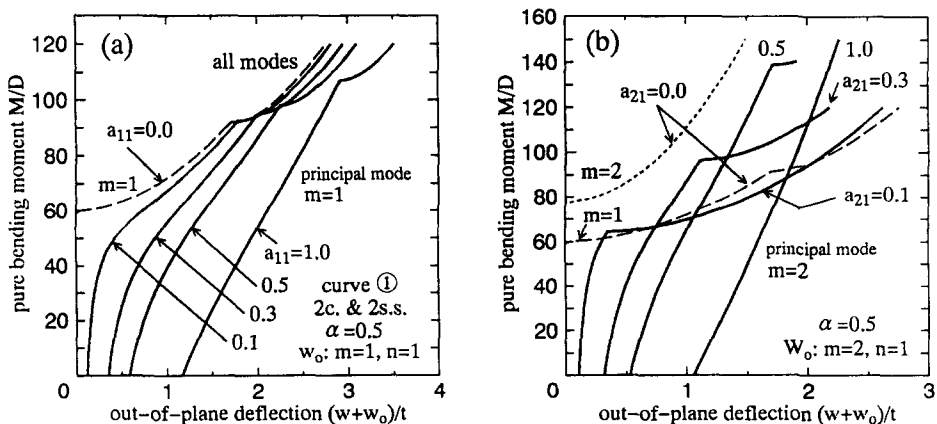

Fig. 8. Effect of initial deflection on a plate of *aspect ratio* $\alpha = 0.5$ under two oppposite sides clamped and the other two sides simply supported condition: (a) imperfection mode of a_{11}; (b) a_{21}.
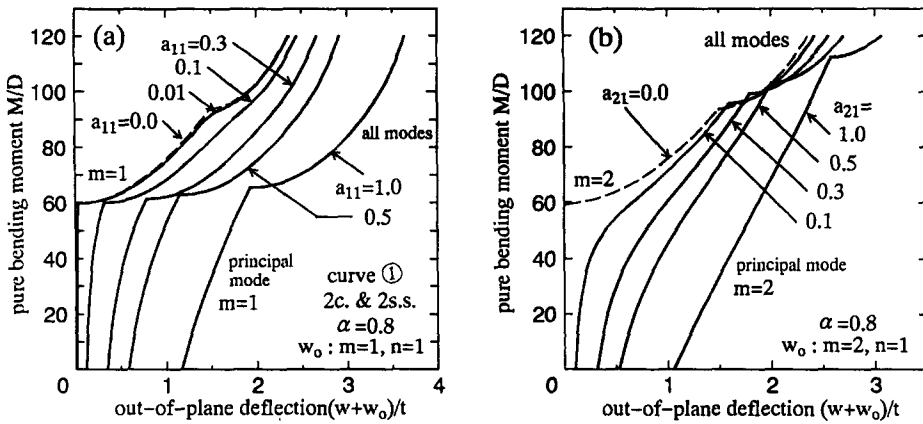
Fig. 9. Effect of initial deflection on a plate of *aspect ratio* $\alpha = 0.8$ under two opposite sides clamped and the other two sides simply supported condition: (a) imperfection mode of a_{11}; (b) a_{21}.

An interesting phenomenon is observed in Fig. 8(b) where the initial deflection mode is a_{21}. The deformation prior to the bifurcation is composed of the principal mode $m = 2$ with minor mode $m = 6$, and the loading level of critical moments is strongly affected by the magnitude of a_{21} and another fundamental path of mode $m = 2$ with no imperfections. However, this fundamental path itself is unstable as shown by a broken line, and thus the stable equilibrium paths other than the mode of $m = 1$ or 2 appear. The configuration of a plate is composed of all the modes mixed above the bifurcation load, but the principal mode remains $m = 2$.

The results of $\alpha = 0.8$ are shown in Fig. 9, where the primary buckling mode is $m = 2$. If the initial deflection mode a_{11} is given, the instability phenomenon of bifurcation type happens at almost the same loading level as the primary buckling and is shown in Fig. 9(a). Firstly, the out-of-plane deformation is composed of the symmetric modes of $m = 1, 3$ and 5, and is similar to that of a sub-panel of the shallow barrel subjected to pure bending moment. In other words, Fig. 9(a) represents the simulation of a non-linear behavior of a curved panel with the mode of $m = 1$ and its bifurcation phenomena. No buckling occurs at higher loading levels as the secondary instability appears after the primary bifurcation.

Other load-deflection curves are shown in Fig. 9(b) when the initial deflection mode is a_{21}. Similar to the case shown in Fig. 8(a), the primary buckling vanishes but the buckling occurs at the same or higher loading level as the secondary bifurcation point of the perfect case.

As described in this section, the instability phenomena of a plate clamped at two opposite sides and simply supported along the other two sides are quite complex and depend on not only the magnitude and mode of the initial deflection but also the shape of the panel.

4. INSTABILITY PHENOMENA UNDER UNEQUAL BENDING AND SHEAR

The type of loading also plays an important role on the buckling phenomena, and the effect of combined loading of shearing forces and bending moments on the secondary buckling is examined here. Figure 10(a) shows a typical example when a simply-supported and perfect plate of $\alpha = 0.8$ is subjected to unequal bending and shear, where the shearing force ratio is fixed as $\omega = 0.1$ and the ratio of the unequal moments γ is varied. When γ is small, namely when the extent of inequality of the bending moments becomes relatively large and thereby the effect of shearing force becomes preferable to that of the bending moments, the snap-through phenomenon is clearly recognized. Another example of $\alpha = 0.75$ and $\omega = 0.133$ can be found in Fig. 6 of the study by Nakazawa *et al.* (1991).

Figure 10(b) shows a similar result of a rectangular plate clamped at two opposite sides and simply supported along the other two sides in the case of $\alpha = 0.5$ and $\omega = 0.1$. The post-buckling paths show two different tendencies depending on the value of γ, and
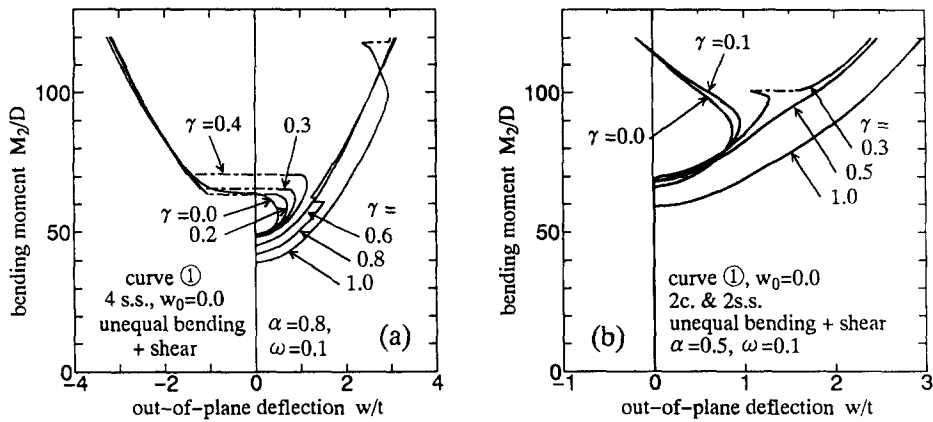
Fig. 10. Post-buckling behavior of a plate under unequal bending and shear: (a) *aspect ratio* $\alpha = 0.8$, $\omega = 0.1$ under simply supported condition; (b) $\alpha = 0.5$, $\omega = 0.1$ under two opposite sides clamped and the other two sides simply supported condition.

5. CONCLUSION

(1) A simply-supported plate exhibits the secondary buckling of the snap-through type when subjected to pure bending, and the mode change of deformed configuration can be classified into three regions in the limited range of this analysis; i.e. from $m = 1$ to 3 in the aspect ratio $\alpha \leqslant 0.98$, $m = 2$ to 3 in $0.98 < \alpha \leqslant 1.65$ and $m = 3$ to 5 in $\alpha > 1.65$. Other similar phenomena will also be obtained as the aspect ratio increases.

(2) When a rectangular plate clamped at two opposite sides and simply supported along the other two sides is subjected to pure bending, the bifurcation-type instability occurs, and the symmetrically deformed configuration changes to the asymmetrical one. After reaching the instability point, all the harmonics of the b_{mn}s contribute to the deformation of a plate in which the rate of these contributions becomes smaller as the order of the mode becomes higher, but the same principal mode as the primary buckling one remains.

(3) The secondary instability is observed at a relatively lower loading level when the aspect ratio lies near the intersection point of the primary buckling curves, especially in the case of a plate with two opposite sides clamped and the other two sides simply supported. Therefore, this secondary instability phenomenon can be likely to occur even in the practical situations of low loading level.

(4) The effect of initial deflection on the secondary buckling is somewhat complex. In the simply-supported case, the existence of the initial deflection of the mode a_{11} slightly increases the secondary buckling load. On the other hand, the higher-order modes of imperfection a_{21} or a_{31} give a stabilizing effect on this secondary instability phenomenon and lead to the monotonically increasing paths except when the imperfection is very small. If two opposite sides are clamped and the other two sides are simply supported, the bifurcation happens even when the initial imperfection exists, and the buckling load level depends on the shape of the panel and the mode of imperfection.

(5) The effect of combined loading also yields another secondary instability and results the mode change of deformed configuration. Some numerical examples exhibit that the secondary buckling phenomenon also happens in the case of combined loading of unequal bending moments and shearing forces.

REFERENCES

Bauer, L. and Reiss, E. L. (1965). Nonlinear buckling of rectangular plates. *J. Soc. Indust. Appl. Math.* **13**(3), 603–626.

Britvec, S. J. (1973). *The Stability of Elastic Systems.* Pergamon Press, New York.

Chilver, A. H. (1967). Coupled modes of elastic buckling. *J. Mech. Phys. Solids* **15**, 15–28.

Coan, J. M. (1951). Large deflection theory for plates with small initial curvature loaded in edge compression. *J. Appl. Mech.* **18**, 143–151.

Fujii, K. and Ohmura, H. (1989). Nonlinear bending behavior of curved girder-web with initial deflections. *JSCE, J. Struct. Engng* **35A**, 117–126 (in Japanese).

Hasegawa, A., Chaisomphob, T. and Iwakuma, T. (1987). An elastic post-buckling behaviour of propped-cantilever column. *Structural Engng/Earthquake Engng JSCE* **4**(1), 221s–224s.

Konishi, I., Shiraishi, N. and Watanabe, E. (1966). A consideration on the strength of webplates. *Proc. JSCE* No. 136, 15–23 (in Japanese).

Kutzelnigg, E. (1978). Beulwertdiagramme für Stegbleche ohne Zwischensteifen nach der linearen Beultheorie bei Berücksichtigung von in Trägerlängsrichtung veränderlichen Spannungen und der Torsionssteifigkeit der Trägergurte. *Der Stahlbau* **J47**(11), 329–338.

Levy, S. (1942). Bending of rectangular plates with large deflections. *NACA, Technical Notes,* No. 846.

Levy, S., Fienup, K. L. and Wooley, R. M. (1945). Analysis of square shear web above buckling load. *NACA, Technical Notes,* No. 962.

Maaskant, R. and Roorda, J. (1992). Mode jumping in biaxially compressed plates. *Int. J. Solids Structures* **29**(10), 1209–1219.

Mikami, I. and Yonezawa, H. (1975). Extrapolation technique for finite difference and finite element solutions. *Theoret. Appl. Mech.* **25**, 567–575.

Moriwaki, Y. and Nara, S. (1989). Buckling strength of web plates of plate girders under in-plane combined loading. *JSCE, J. Struct. Engng* **35A**, 127–134 (in Japanese).

Nakamura, T. and Uetani, K. (1979). The secondary buckling and post-secondary-buckling behaviours of rectangular plates. *Int. J. Mech. Sci.* **21**, 265–286.

Nakazawa, M., Iwakuma, T. and Kuranishi, S. (1991). Elastic buckling strength and post-buckling behavior of a panel under unequal bending and shear. *Structural Engng/Earthquake Engng JSCE* **8**(1), 11s–20s.

Salvadori, M. G. (1951). Numerical computation of buckling loads by finite differences. *Trans. ASCE* **116**, 590–624.

Salvadori, M. G. and Baron, M. L. (1961). *Numerical Methods in Engineering* (2nd Edn). Prentice-Hall, Englewood Cliffs, New Jersey.

Sharman, P. W. and Humpherson, J. (1968). An experimental and theoretical investigation of simply-supported thin plates subjected to lateral load and uniaxial compression. *Aeronaut. J. Roy. Aeronaut. Soc.* **72**, 431–436.

Supple, W. J. (1967). Coupled branching configurations in the elastic buckling of symmetric structural systems. *Int. J. Mech. Sci.* **9**, 97–112.

Supple, W. J. (1968). On the change in buckle pattern in elastic structures. *Int. J. Mech. Sci.* **10**, 737–745.

Supple, W. J. (1970). Changes of wave-form of plates in the post-buckling range. *Int. J. Solids Structures* **6**, 1243–1258.

Thompson, J. M. T. and Hunt, G. W. (1973). *A General Theory of Elastic Stability.* Wiley, New York.

Thompson, J. M. T. and Hunt, G. W. (1984). *Elastic Stability Phenomena.* Wiley, New York.

Timoshenko, S. P. and Goodier, J. N. (1970). *Theory of Elasticity* (3rd Edn). McGraw-Hill, New York.

Uemura, M. and Byon O-Il (1977). Secondary buckling of a flat plate under uniaxial compression. Part 1: Theoretical analysis of simply supported flat plate. *Int. J. Non-Lin. Mech.* **12**, 355–370.

Uemura, M. and Byon O-Il (1978). Secondary buckling of a flat plate under uniaxial compression. Part 2: Analysis of clamped plate by F.E.M. and comparison with experiments. *Int. J. Non-Lin. Mech.* **13**, 1–14.

Usami, T. (1982). Post-buckling of plates in compression and bending. *ASCE, J. Struct. Div.* **108**, No. ST3, 591–609.

Yamaki, N. (1959). Postbuckling behavior of rectangular plates with small initial curvature loaded in edge compression. *Trans. ASME, J. Appl. Mech.* **26**, 407–414.